Electronic supplementary information (ESI) for the manuscript:

Insight into the effect of incorporation of boron in ZSM-11 on its catalytic performance for conversion of methanol to olefins

Sen Wang [a,b,†], Shiying Li [a,b,†], Li Zhang [a,b], Zhangfeng Qin [a], Mei Dong [a], Junfen Li [a], Jianguo Wang [a], Weibin Fan [a,*]

[a] *State Key Laboratory of Coal Conversion, Institute of Coal Chemistry, Chinese Academy of Sciences, 27 South Taoyuan Road, Taiyuan, Shanxi 030001, PR China*

[b] *University of Chinese Academy of Sciences, Beijing 100049, PR China*

[†] *These authors equally contributed to this work*

[*] *Corresponding author. Tel.: +86-351-4199009; Fax: +86-351-4041153*

E-mail address: fanwb@sxicc.ac.cn

Table of contents:

the alkene cycle of MTO process catalyzed by H-ZSM-11.

Table S5. Calculated ^{27}Al NMR shielding tensors (δ_{ST}, ppm) and chemical shifts (δ_{CS}, ppm) of different T sites over ZSM-11.

Table S6. Distributions of different types of Al species in AlZSM-11 and [B,Al]ZSM-11 with different B/Al ratios, as measured by DR UV-vis spectroscopy after being exchanged with Co^{2+}.

Figure captions

Fig. S1. Cluster models of AlZSM-11 (a) and [B,Al]ZSM-11 (b).

Fig. S2. XRD patterns of AlZSM-11 (a) and [B,Al]ZSM-11 with B/Al ratio of (b) 1.0; (c) 2.0 and (d) 8.0.

Fig. S3. SEM images of AlZSM-11 (a) and [B,Al]ZSM-11 with B/Al ratio of (b) 1.0; (c) 2.0 and (d) 8.0.

Fig. S4. Nitrogen adsorption/desorption isotherms of AlZSM-11 and [B,Al]ZSM-11 with different B/Al ratios.

Fig. S5. Framework IR spectra of AlZSM-11 (a) and [B,Al]ZSM-11 with different B/Al ratios.

Fig. S6. Py-IR spectra collected at 423 K of AlZSM-11 (a) and [B,Al]ZSM-11 with B/Al ratio of (b) 1.0; (c) 2.0 and (d) 8.0.

Fig. S7. Proposed aromatic and alkene cycles of MTO process catalyzed by H-ZSM-11.

Fig. S8. Periodic model of silicalite-2 (pure-silica ZSM-11) (a); optimized AlZSM-11 structure with Al substituting Si at T1 site and charge-compensating Na^+ cation located at O8 (b) and O9 (c).

Fig. S9. Optimized AlZSM-11 structure with Al substituting Si at T2, T3 and T4 site, respectively.

Fig. S10. Optimized AlZSM-11 structure with Al substituting Si at T5, T6 and T7 site, respectively.

Fig. S11. ^{27}Al MAS NMR spectra of calcined AlZSM-11 (a) and [B,Al]ZSM-11 with B/Al ratio of (b) 1.0; (c) 2.0 and (d) 8.0.

Fig. S12. Relationship between catalytic lifetimes of AlZSM-11 and [B,Al]ZSM-11 with different B/Al ratios and the area of the signal around 53.8 ppm in ^{27}Al MAS NMR spectra.

Table S1. Calculated proton affinity (PA) and ammonia adsorption energies (ΔE_{ads}) of the acid sites in AlZSM-11 and [B,Al]ZSM-11.

Models	PA (kJ mol^{-1})	ΔE_{ads} (kJ mol^{-1})
AlZSM-11	1104	–166
[B,Al]ZSM-11	1111	–157

Table S2. The contents of Brönsted (μmol g^{-1}) and Lewis acid sites (μmol g^{-1}) of AlZSM-11 and [B,Al]ZSM-11 with different B/Al ratios, as measured by Py-IR at different temperature.

Zeolites	Py-IR (423 K) [a]		Py-IR (523 K) [a]		Py-IR (623 K) [a]	
	Brönsted	Lewis	Brönsted	Lewis	Brönsted	Lewis
B/Al=0.0	42	17	37	8	32	6
B/Al=1.0	59	21	45	6	33	6
B/Al=2.0	80	25	42	5	34	5
B/Al=8.0	117	17	48	6	36	4

[a] The contents of Brönsted and Lewis acid sites determined by Py-IR with the amounts of pyridine (Py) desorbed at 423, 523 and 623 K, respectively.

Table S3. Calculated free energy barriers ($\Delta G_{\mathrm{int}}^{\neq}$), relative rate constants (k), enthalpy barriers ($\Delta H_{\mathrm{int}}^{\neq}$) and entropy losses ($-T\Delta S_{\mathrm{int}}^{\neq}$) at 723 K of each reaction step in the aromatic cycle of MTO process catalyzed by H-ZSM-11.

	$\Delta G_{\mathrm{int}}^{\neq}$ (kJ mol^{-1})	k (s^{-1})	$\Delta H_{\mathrm{int}}^{\neq}$ (kJ mol^{-1})	$-T\Delta S_{\mathrm{int}}^{\neq}$ (kJ mol^{-1})
AlZSM-11				
M0	96	1.66×10^{6}	97	–1
M1	119	3.68×10^{4}	98	21
M2	54	2.00×10^{9}	48	6
M3	67	2.01×10^{8}	56	11
D1	64	3.50×10^{8}	54	10
D2	98	1.32×10^{6}	80	18
E1	207	1.59×10^{-2}	195	12
[B,Al]ZSM-11				
M0	100	9.02×10^{5}	106	–6
M1	123	1.87×10^{4}	107	16
M2	53	2.31×10^{9}	46	7
M3	72	9.22×10^{7}	58	14
D1	60	7.61×10^{8}	57	3
D2	74	6.78×10^{7}	58	16
E1	195	1.34×10^{-1}	192	3

Note: only one acid site generated by replacing Al with Si at T1 site and locating charge-balancing proton at O9 over AlZSM-11, and two acid sites generated by replacing two Si atoms with one Al and one B atoms at adjacent T1 sites and locating two charge-balancing protons at O9 ions connected to Al and B, respectively, over [B,Al]ZSM-11 (only the acid site resulted from incorporation of Al catalyze the MTO reaction).

Table S4. Calculated free energy barriers ($\Delta G_{\text{int}}^{\neq}$), relative rate constants (k), enthalpy barriers ($\Delta H_{\text{int}}^{\neq}$) and entropy losses ($-T\Delta S_{\text{int}}^{\neq}$) at 723 K of each reaction step in the alkene cycle of MTO process catalyzed by H-ZSM-11.

	$\Delta G_{\text{int}}^{\neq}$ (kJ mol^{-1})	k (s^{-1})	$\Delta H_{\text{int}}^{\neq}$ (kJ mol^{-1})	$-T\Delta S_{\text{int}}^{\neq}$ (kJ mol^{-1})
AlZSM-11				
M0	96	1.66×10^{6}	97	–1
M1	86	9.64×10^{6}	60	26
M2	78	3.73×10^{7}	54	24
M3	82	1.86×10^{7}	69	13
D1	41	1.58×10^{10}	52	–11
D2	44	1.08×10^{10}	56	–12
E1	96	1.79×10^{6}	132	–36
[B,Al]ZSM-11				
M0	100	9.02×10^{5}	106	–6
M1	80	2.32×10^{7}	61	19
M2	76	4.67×10^{7}	58	18
M3	88	6.55×10^{6}	69	19
D1	43	1.14×10^{10}	56	–13
D2	65	2.75×10^{8}	69	–4
E1	111	1.46×10^{5}	142	–31

Note: only one acid site generated by replacing Al with Si at T1 site and locating charge-balancing proton at O9 over AlZSM-11, and two acid sites generated by replacing two Si atoms with one Al and one B atoms at adjacent T1 sites and locating two charge-balancing protons at O9 ions connected to Al and B, respectively, over [B,Al]ZSM-11 (only the acid site resulted from incorporation of Al catalyze the MTO reaction).

Table S5. Calculated ^{27}Al NMR shielding tensors (δ_{ST}, ppm) and chemical shifts (δ_{CS}, ppm) of different T sites over ZSM-11.

T sites	Shielding tensors (δ_{ST}) [a]	Chemical shifts (δ_{CS}) [b]
T1	532.2	54.7
T2	530.4	56.5
T3	540.3	46.6
T4	529.8	57.1
T5	521.7	65.2
T6	529.9	57.0
T7	537.8	49.1

[a] B3LYP/6-31G (d, p) method was adopted for geometry optimization of different T sites based on the 40T cluster models and B3LYP/DGDZVP with GIAO method was used for ^{27}Al NMR shielding tensors calculation.[1,2]

[b] The chemical shift of ^{27}Al NMR is obtained by the difference between the calculated chemical shift of $Al(H_2O)_6^{3+}$ (586.9 ppm) and the shielding tensors of different T sites, viz., $\delta_{CS} = 586.9 - \delta_{ST}$.[3]

Table S6. Distributions of different types of Al species in AlZSM-11 and [B,Al]ZSM-11 with different B/Al ratios, as measured by DR UV-vis spectroscopy after being exchanged with Co^{2+}.

Zeolites	Al_{close} (%) [a]	Al_{single} (%) [a]	$\alpha+\gamma$ type (%) [b]	β type (%) [b]
B/Al=0.0	57.1	42.9	56.5	43.5
B/Al=1.0	56.0	44.0	51.9	48.1
B/Al=2.0	65.7	34.3	40.4	59.6
B/Al=8.0	63.5	36.5	34.8	65.2

[a] The fraction of Al_{close} or Al_{single} was calculated with the equations of $[Al_{close}]=2\times[Co_{max}]$ and $[Al_{single}]=[Al_{total}]-2\times[Co_{max}]$, respectively. $[Al_{total}]$ and $[Co_{max}]$ are the contents of Al and Co atoms in the Co^{2+}-exchanged zeolites, as measured by the ICP-AES technique.

[b] The distribution of various types (α, β, and γ) of Co^{2+} ions was determined by the deconvolution of DR UV-vis spectra of Co^{2+}-exchanged ZSM-11 zeolites.

Fig. S1.

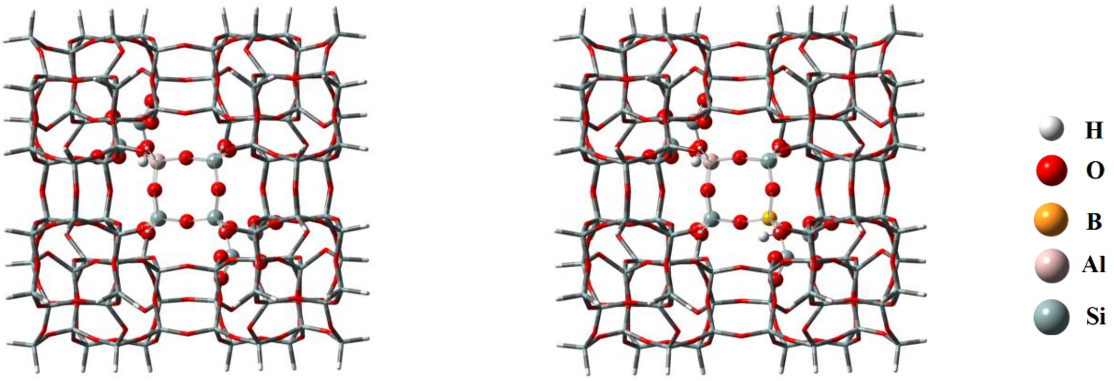

(a) (b)

Fig. S1. Cluster models of AlZSM-11 (a) and [B,Al]ZSM-11 (b). Only one acid site generated by replacing Al with Si at T1 site and locating charge-balancing proton at O9 over AlZSM-11, and two acid sites generated by replacing two Si atoms with one Al and one B atoms at adjacent T1 sites and locating two charge-balancing protons at O9 ions connected to Al and B, respectively, over [B,Al]ZSM-11 (only the acid site resulted from incorporation of Al catalyze the MTO reaction).

Fig. S2.

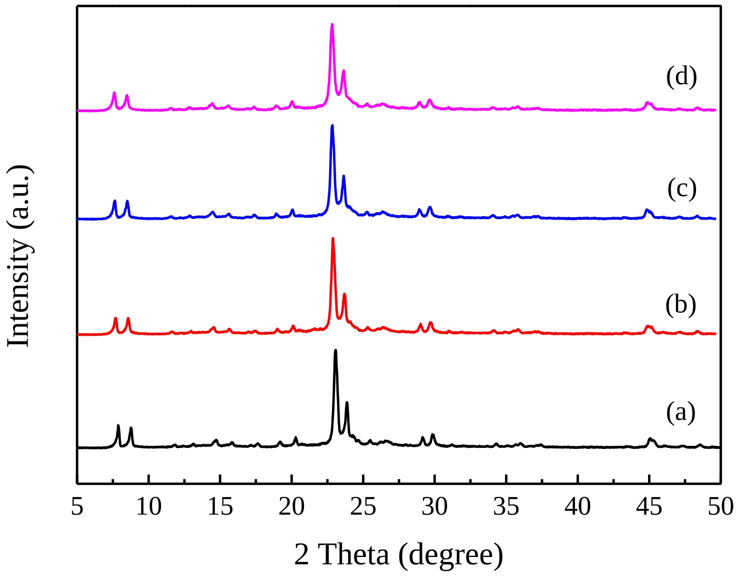

Fig. S2. XRD patterns of AlZSM-11 (a) and [B,Al]ZSM-11 with B/Al ratio of (b) 1.0; (c) 2.0 and (d) 8.0.

Fig. S3.

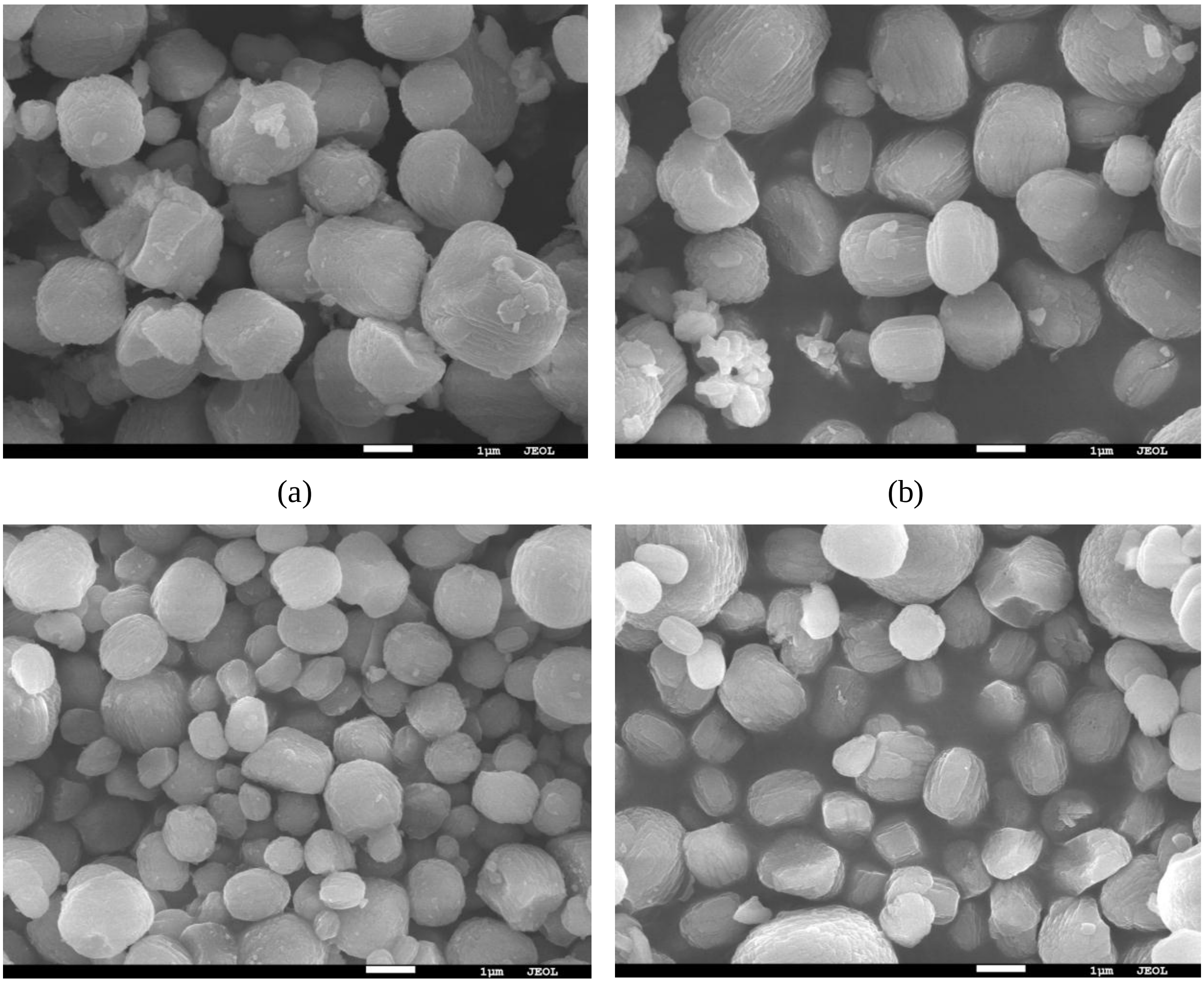

(a) (b)

(c) (d)

Fig. S3. SEM images of AlZSM-11 (a) and [B,Al]ZSM-11 with B/Al ratio of (b) 1.0; (c) 2.0 and (d) 8.0.

Fig. S4.

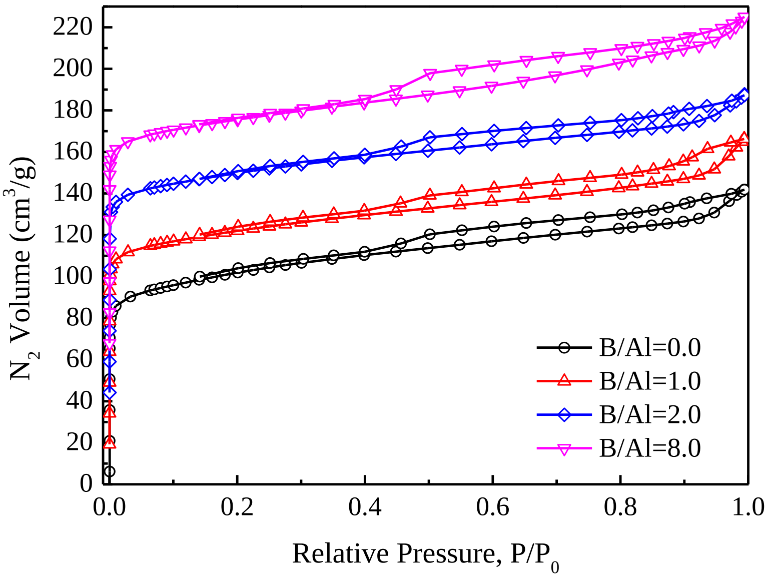

Fig. S4. Nitrogen adsorption/desorption isotherms of AlZSM-11 and [B,Al]ZSM-11 with different B/Al ratios.

Fig. S5.

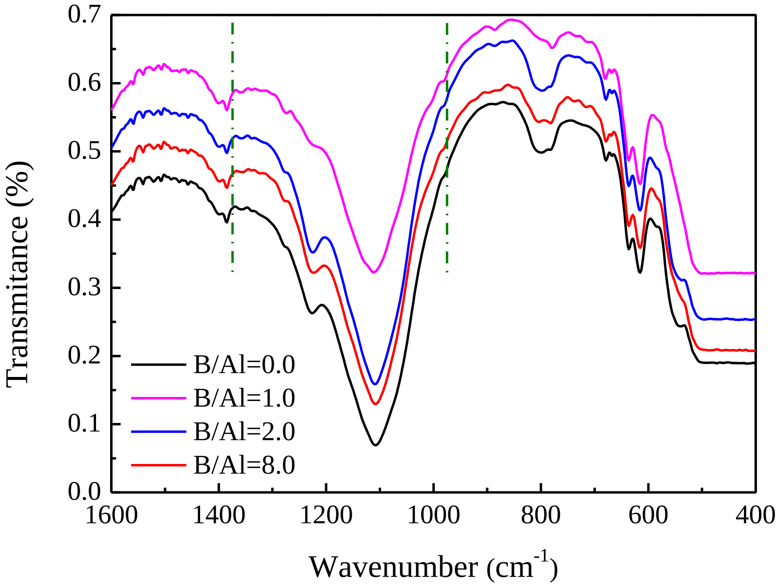

Fig. S5. Framework IR spectra of AlZSM-11 (a) and [B,Al]ZSM-11 with different B/Al ratios.

Fig. S6.

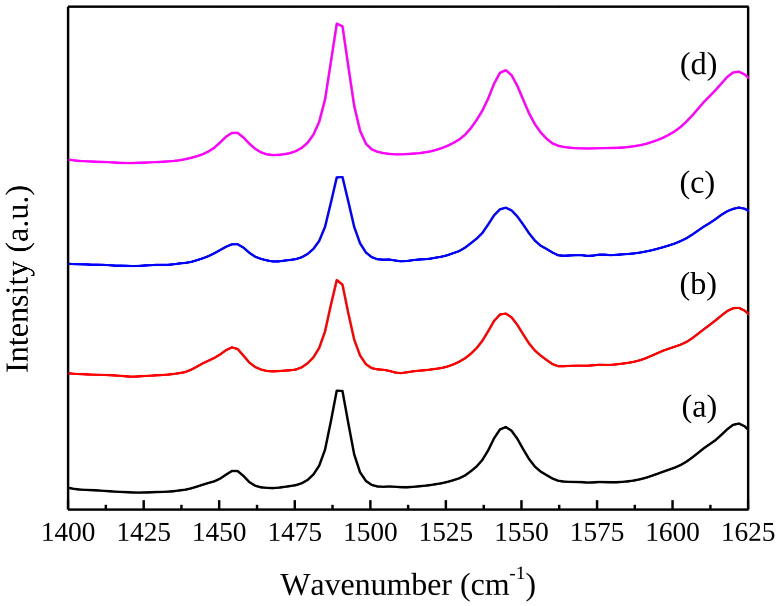

Fig. S6. Py-IR spectra collected at 423 K of AlZSM-11 (a) and [B,Al]ZSM-11 with B/Al ratio of (b) 1.0; (c) 2.0 and (d) 8.0.

Fig. S7.

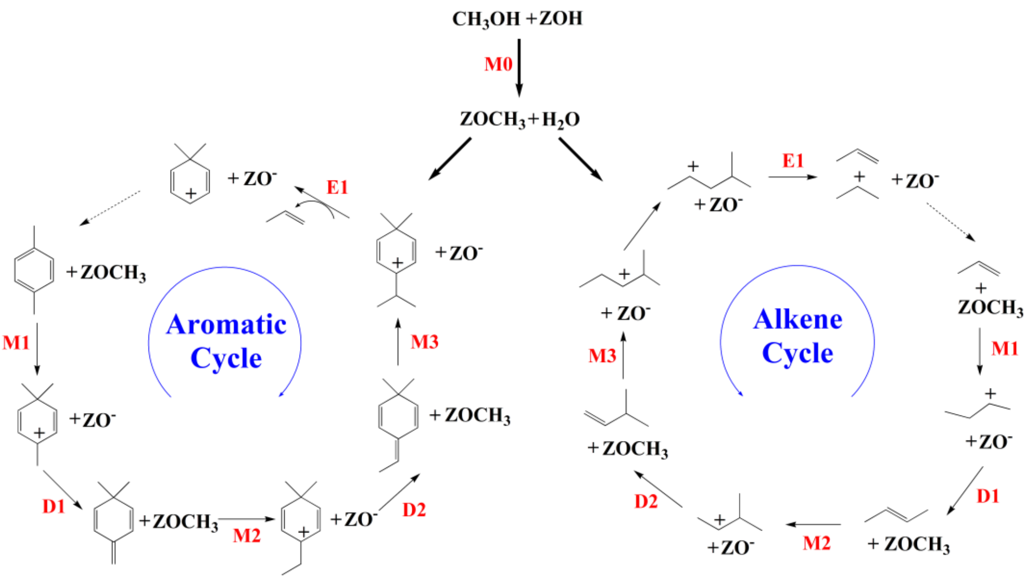

Fig. S7. Proposed aromatic and alkene cycles in MTO process catalyzed by H-ZSM-11.

Fig. S8.

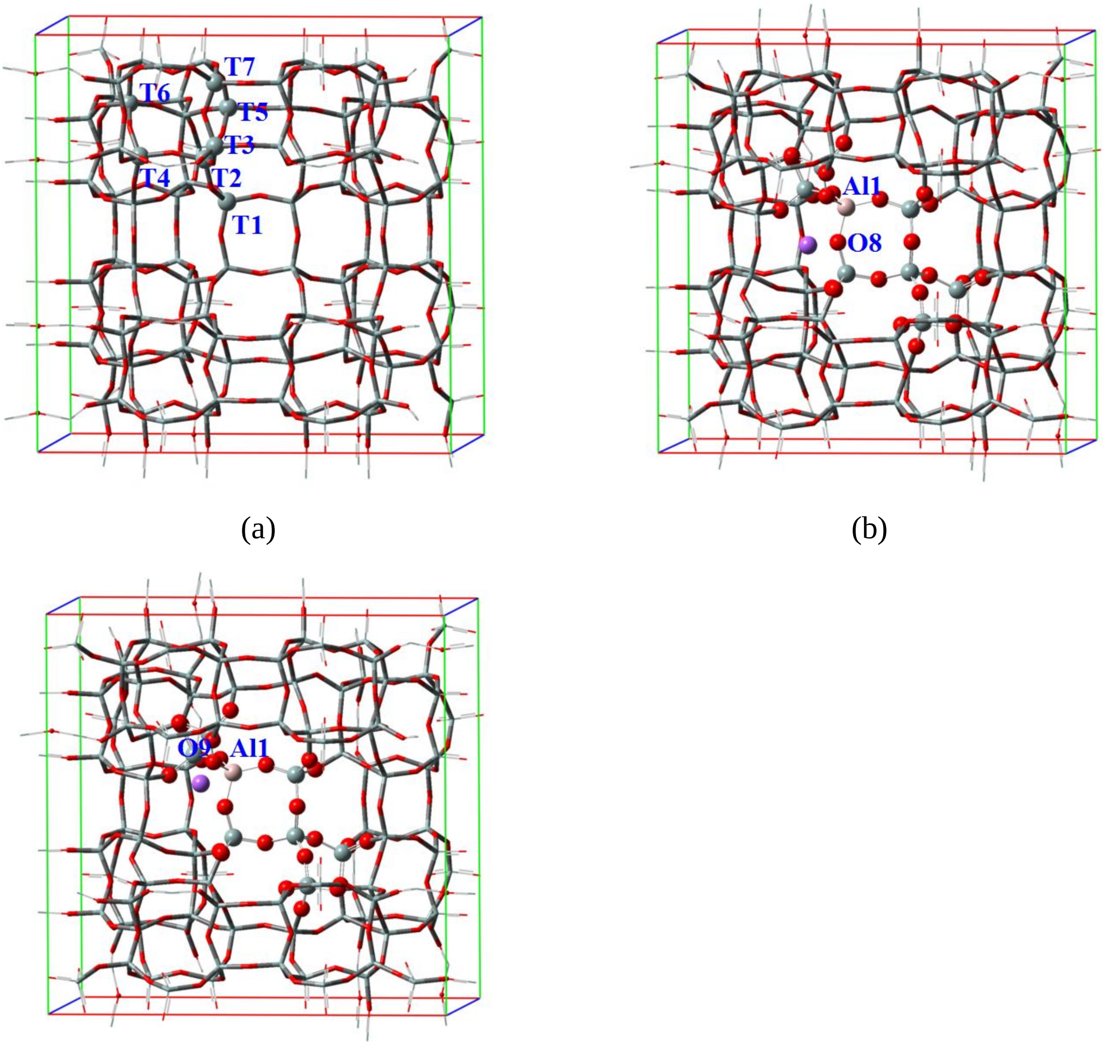

(a) (b)

(c)

Fig. S8. Periodic model of silicalite-2 (pure-silica ZSM-11) (a); optimized AlZSM-11 structure with Al substituting Si at T1 site and charge-compensating Na^+ cation located at O8 (b) and O9 (c) (grass: Si; red: O; pink: Al; purple, Na^+).

Fig. S9.

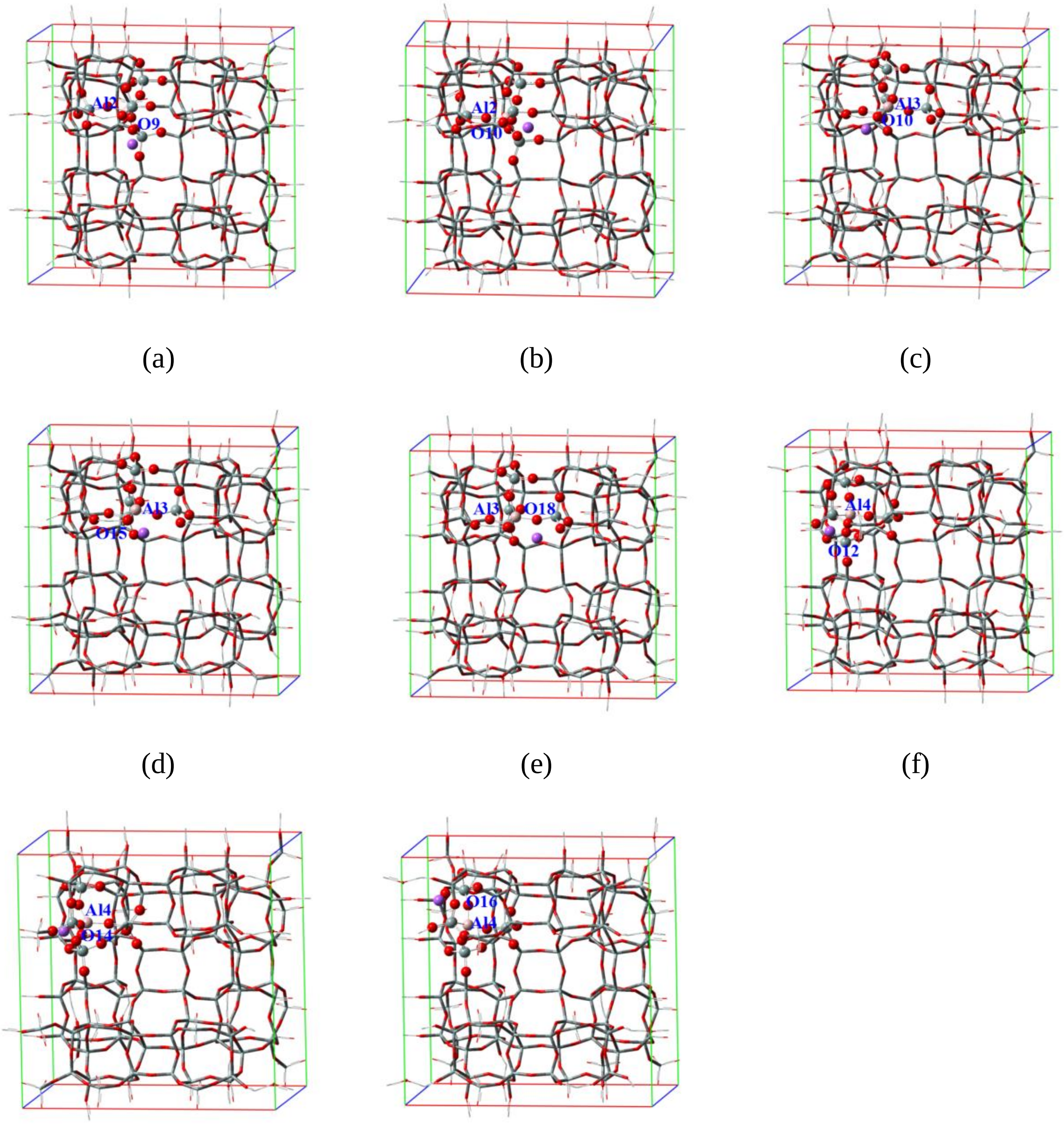

(a) (b) (c)

(d) (e) (f)

(g) (h)

Fig. S9. The optimized AlZSM-11 structure with Al substituting Si at T2, T3 and T4 site, respectively (grass: Si; red: O; pink: Al; purple, Na^+).

Fig. S10.

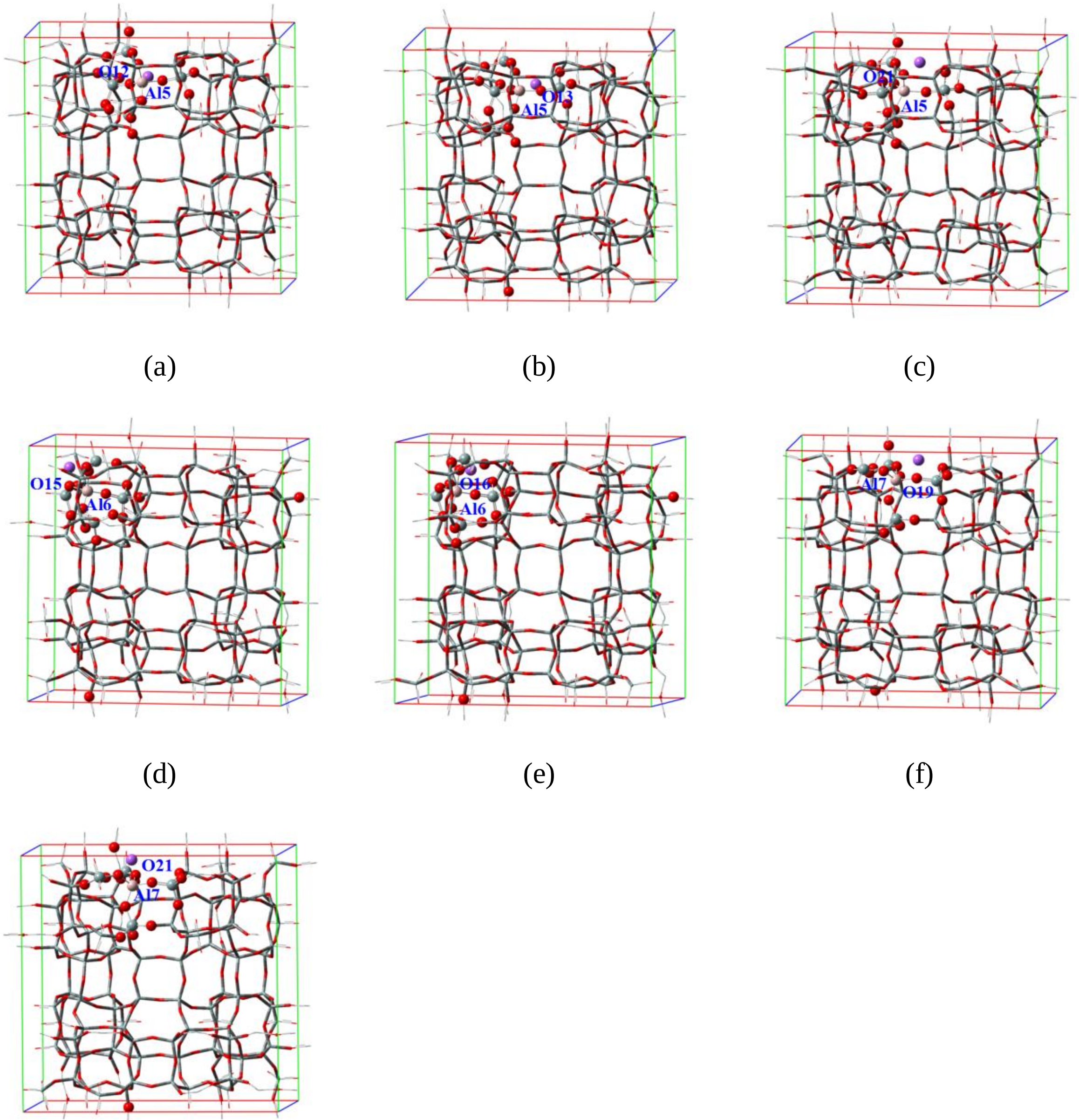

(a) (b) (c)

(d) (e) (f)

(g)

Fig. S10. The optimized AlZSM-11 structure with Al substituting Si at T5, T6 and T7 site, respectively (grass: Si; red: O; pink: Al; purple, Na^+).

Fig. S11.

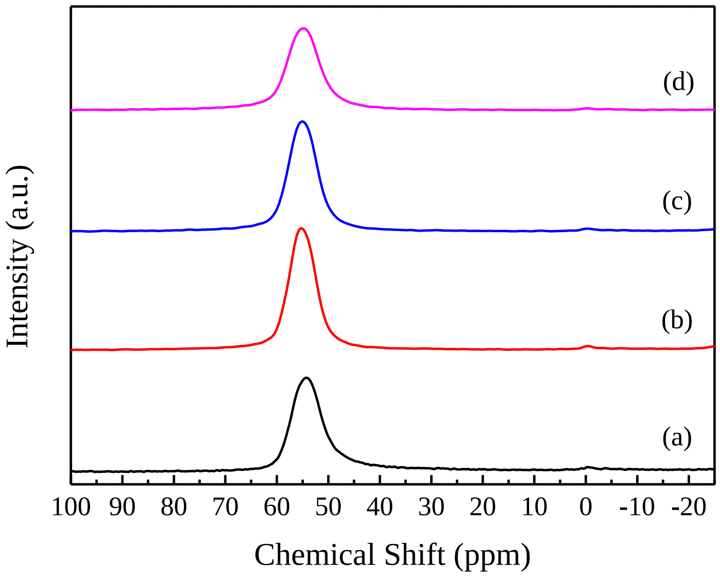

Fig. S11. ^{27}Al MAS NMR spectra of calcined AlZSM-11 (a) and [B,Al]ZSM-11 with B/Al ratio of (b) 1.0; (c) 2.0 and (d) 8.0.

Fig. S12.

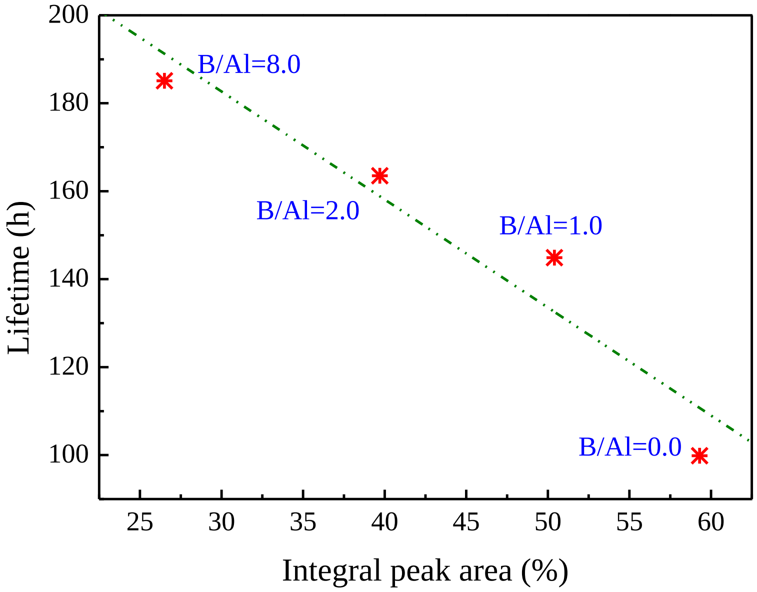

Fig. S12. Relationship between catalytic lifetimes of AlZSM-11 and [B,Al]ZSM-11 with different B/Al ratios and the area of the signal around 53.8 ppm in ^{27}Al MAS NMR spectra.

(1) K. Wolinski, J. F. Hinton and P. Pulay, *J. Am. Chem. Soc.*, 1990, **112**, 8251–8260.

(2) R. R. Zhao, Z. C. Zhao, S. K. Li and W. P. Zhang, *J. Phys. Chem. Lett.*, 2017, **8**, 2323−2327.

(3) A.Vjunov, J. L. Fulton, T. Huthwelker, S. Pin, D. H. Mei, G. K. Schenter, N. Govind, D. M. Camaioni, J. Z. Hu and J. A. Lercher, *J. Am. Chem. Soc*., 2014, **136**, 8296−8306.